

Effects of annealing on plasma-deposited a -Si:H films grown under optimal conditions

B. A. Wilson, A. M. Sergent, K. W. Wecht, A. J. Williams, and T. P. Kerwin
AT&T Bell Laboratories, Murray Hill, New Jersey 07974

C. M. Taylor and J. P. Harbison

Bell Communications Research, Inc., Murray Hill, New Jersey 07974

(Received 2 December 1983; revised manuscript received 1 May 1984)

A comprehensive study is presented of the effects of isochronal annealing on the optical properties, spin density, and hydrogen evolution of plasma-deposited a -Si:H films grown under optimal conditions. In contrast to studies covering a wide range of growth parameters, purely monotonic behavior is observed in most of the properties of these films for annealing temperatures from 300 to 600°C. While changes in the optical gap parallel the hydrogen content of the films, the quenching of the main luminescence band more closely reflects the spin density. Two quenching processes, occurring on very different time scales, are observed in time-resolved measurements of this band. Both depend on spin density, and are modeled as two different trapping mechanisms at dangling-bond defects. An additional luminescence band peaking at about 0.7 eV is studied, which is enhanced by annealing up to 525°C, and quenched above. The ratio of intensities in the two bands scales linearly with spin density, and we propose that the 0.7-eV band represents radiative recombination between an electron in a conduction-band-tail state and a hole trapped at a dangling bond. We present a simple quantitative model of the competing radiative and nonradiative processes that self-consistently accounts for the observed cw and time-resolved optical properties of both bands. These results are compared with a variety of other measurements in amorphous and microcrystalline Si.

I. INTRODUCTION

The evolution in the properties of a -Si:H films subjected to a progression of high-temperature anneals provides insight into basic questions of composition, bonding, and electronic states in these materials. In particular, studies of the temperatures at which hydrogen is emitted from the sample, and of the changes in spin density and optical characteristics associated with this process, provide direct information on the role of hydrogen in the optical and electronic properties of a -Si:H. Previous studies¹⁻¹² have examined the effects of annealing on samples with a broad range of deposition parameters, emphasizing the differences due to sample-preparation conditions. These studies, supported by other measurements, have defined growth parameters which produce the highest-quality materials. Such high-quality films are characterized by electronic properties that allow some of the same applications as for crystalline semiconductors. In this paper we focus specifically on these technologically useful materials grown under close to optimal conditions. We present a comprehensive study of the effects of annealing on the optical properties, and relate these effects to the spin density and hydrogen content of the films.

The temperature range for sample annealing was taken from slightly above the anode temperature used during growth (250°C) to a temperature known to produce complete hydrogen evolution² (about 650°C). Two sets of annealing experiments were performed. In the first a number of different samples grown at different $[\text{SiH}_4]/[\text{Ar}]$ gas ratios were each subjected to a series of 20-min an-

neals at 25°C temperature intervals. This provided a comprehensive picture of the pattern of spin creation and hydrogen evolution with annealing in these films. In the second set of experiments identical samples (i.e., films grown simultaneously) were annealed separately, each at a different temperature. The hydrogen evolution and spin densities were found to follow the same pattern as for progressively annealed films.

Optical measurements including absorption, cw luminescence, time-resolved luminescence, and Raman scattering were subsequently performed on these films and the optical properties correlated with hydrogen evolution and spin density. In an earlier paper¹³ we reported the behavior of the main luminescence band and of the narrower band at 0.7 eV as a function of spin density, and presented a model of the dynamics leading to recombination in these two bands. In this paper we examine this model in more detail and compare the results with other measurements in these materials.

II. EXPERIMENTAL TECHNIQUES

A. Sample preparation

Fused quartz substrates used in this experiment were cut into 5 mm × 5 mm squares from 10-mil-thick sheets. After cutting, the pieces were etched for 5 min in a solution of distilled H₂O (30 cm³), HNO₃ (15 cm³) and HF (2 cm³), then washed in hot distilled H₂O and dried. Films of undoped a -Si:H were plasma-deposited from high-purity SiH₄ in Ar onto the quartz substrates. For the pro-

gressive annealing experiments, six runs were made with gas concentration (volume percentage of SiH₄ in Ar) ranging from 3 to 100 vol %. Substrates were held at 250°C for each film deposition. For the experiments measuring the optical properties after single temperature anneals, ten films were grown simultaneously on roughened fused silica substrates at a gas ratio of 10 vol % SiH₄. The 13.5-MHz power level was set at 5 W capacitively coupled into plates 5 cm in diameter with a 1.5-cm spacing. No apparent dc bias was present. The gas flow through the system metered by precision flow meters was 50 standard cubic centimeters per minute for all seven runs. The deposition pressures were all in the range 0.36–0.49 Torr and are listed in Table I together with the other sample characteristics. Included are the growth rates, which depend on both the deposition pressure and the SiH₄ dilution ratio. The film thicknesses were measured using a scanning electron microscope (SEM), and varied from 0.64 to 2.39 μm .

Our samples were positioned on the anode plate of the system during growth. This has been shown in other studies, using mass spectroscopy, to produce samples that have no detectable argon and evolve only hydrogen when annealed.^{2,5} Relatively thin samples were chosen to minimize columnar growth and structural defects on the sample morphology.¹² Thin films were also chosen to prevent separation of the *a*-Si:H film from the quartz substrate during high-temperature anneals. This was particularly important for the samples grown at high-dilution gas ratios, where recent work¹⁴ has revealed higher levels of stress in the films.

B. Annealing procedures and measurement of hydrogen evolution and electron-spin resonance

For annealing, the sample was placed in a chamber which was originally evacuated to below 2×10^{-5} Torr. The chamber was sealed during the anneal of the sample. The hydrogen evolution was calculated from the measured rise in pressure after correcting for the rise due to the simultaneous outgassing of the chamber itself. For the progressive annealing experiments the sample was removed from the system after each 20-min anneal for ESR measurements. This entire process was repeated at intervals of 25°C beginning at 300°C and terminating at either 650 or 675°C. For the samples annealed at a single tem-

perature, each of seven of the ten identical films was annealed for 20 min as described above at one of the following temperatures: 300, 400, 500, 525, 550, 570, and 600°C. Two samples were measured as-grown, and the final identical film was annealed at 500°C in the same manner, but for a period of 4 h. The hydrogen evolution from these samples was measured by the same procedure, and the samples were removed from the furnace for ESR and optical measurements.

The spin signal was measured at room temperature with a Varian Associates E-4 ESR spectrometer. A modulation field of 12.5 G peak-to-peak amplitude at 100 kHz was typically used for maximum sensitivity. Linewidth measurements were made with a 1- or 2-G amplitude. The signal-to-noise ratio was also optimized by using rather a large microwave power (20 mW). The absolute spin density of each sample was calibrated against a Varian Associates strong-pitch standard source of 10^{15} spins.

C. Optical measurements

A number of cw and pulsed optical measurements were performed on the films annealed at single temperatures. Room-temperature absorption measurements were taken with a standard ir spectrophotometer. The cw luminescence spectra were excited with the 5145-Å line of an argon-ion laser and detected with cooled Ge and InAs photodiodes using lock-in techniques. The spectral range of the two detection systems overlapped in the (0.8–1.0)-eV region, permitting continuous spectral data from 0.6 to 1.65 eV. Since *a*-Si:H has long-lived photoluminescence (PL) components, the chopper for lock-in detection was placed in the collection optics rather than in the exciting beam. In this way the true cw PL was monitored with no loss of contributions from long-lived states. The spectra were corrected for the response of the monochromator and diode detection systems. Absolute quantum efficiencies are very difficult to measure with any accuracy for samples grown on roughened substrates. Consequently, the data presented here are given only as relative efficiencies. Although there is some evidence that the cw quantum efficiencies of similar films approach unity,¹ attempts in our laboratory to measure the integrated efficiency of high-quality films such as these after pulsed ex-

TABLE I. Sample characteristics.

Sample	SiH ₄ (vol %)	<i>d</i> (μm)	Growth rate ($\text{\AA}/\text{s}$)	Deposition pressure (Torr)	Total hydrogen evolved (at. %)	(10^{21} cm^{-3})	Maximum spin density (10^{19} cm^{-3})
1	100	0.64	3.6	0.48	10.1	5.03	2.52
2	30	0.71	3.9	0.44	12.7	6.34	1.43
3	10	2.05	2.9	0.36	18.3	9.15	1.6
4	10	1.28	7.1	0.49	15.4	7.73	1.67
5	3	2.39	3.3	0.36	20.8	10.4	1.33
6	3	1.12	6.2	0.41	13.0	6.53	1.43
7 (A–J)	10	1.4	3.9	0.36	Identical samples annealed at different temperatures		

citation have resulted in considerably smaller estimates on the order of 10%.

Pulsed PL measurements were taken with 15-ns excitation pulses from a frequency-doubled Nd:YAG (neodymium:yttrium-aluminum-garnet) laser (5320 Å) and Ge photodiode detection. The Ge-diode response varies by only ~30% across the main PL band. Thus by inserting a long-pass filter in the collection optics to eliminate scattered laser light, a good approximation of the spectrally integrated decay of the main PL band is obtained. The luminescence band observed at 0.7 eV makes little contribution to these measurements as the Ge responsivity falls rapidly below 0.75 eV. To study the decay of the 0.7-eV band, a long-pass filter transmitting below 0.78 eV was used in the collection optics. For both cw and pulsed PL measurements, the samples were placed in a temperature-controlled flowing-He-gas optical cryostat.

Exposure to intense light, especially at room temperature and above, is known to induce additional spins in *a*-Si:H associated with the Staebler-Wronski effect.^{15,16} Consequently, we have taken care to avoid exposure of our samples to intense laser light at noncryogenic temperatures. Even at low temperatures, we observe some degradation of the photoluminescence quantum efficiency after long, intense exposure, requiring that data collection be carried out with minimal exposure. Since the data scale consistently with the spin densities measured prior to optical excitation, the effects of exposure appear to have no significant effect on the results presented here.

III. HYDROGEN EVOLUTION AND DEFECT CREATION WITH PROGRESSIVE ANNEALING

Figure 1(a) shows the atomic percent of hydrogen evolved at each temperature after a 20-min anneal for four samples in which the ratio of SiH₄ to Ar in the plasma was varied from 3 to 100 vol % SiH₄. The growth rates for these films varied from 3.6 to 7.1 Å/s, but the films are all thin, $0.6 \leq d \leq 1.3 \mu\text{m}$. The shapes of the evolution peaks in the temperature range 450–550°C are roughly the same. Figure 2 is a comparison of the atomic percent of hydrogen evolved at each anneal temperature for two 3-vol % SiH₄ films, samples 5 and 6, whose thicknesses and growth rates differ by a factor of ~2 (1.12 μm at 6.2 Å/s versus 2.39 μm at 3.3 Å/s). The appearance of a second peak between 300 and 400°C in only one of the films clearly shows that even the qualitative shape of the evolution curves can vary as a function of parameters such as growth rate or thickness, even when these parameters are within ranges which yield high-quality materials. The SiH₄ dilution ratio also plays a role since samples 3 and 4, which have growth rates and thicknesses comparable to samples 5 and 6, but were grown at 10 vol % SiH₄ to Ar, show no appearance of the low-temperature peak in either film. The evolution of hydrogen in this low-temperature region has been found to be diffusion-limited.¹⁰ The more rapid release observed here in thicker films grown at very low SiH₄ dilution ratios may be indicative of a more porous structure. In order to avoid materials with these unique properties, thin films grown at 10 vol % dilution ratio were chosen for the

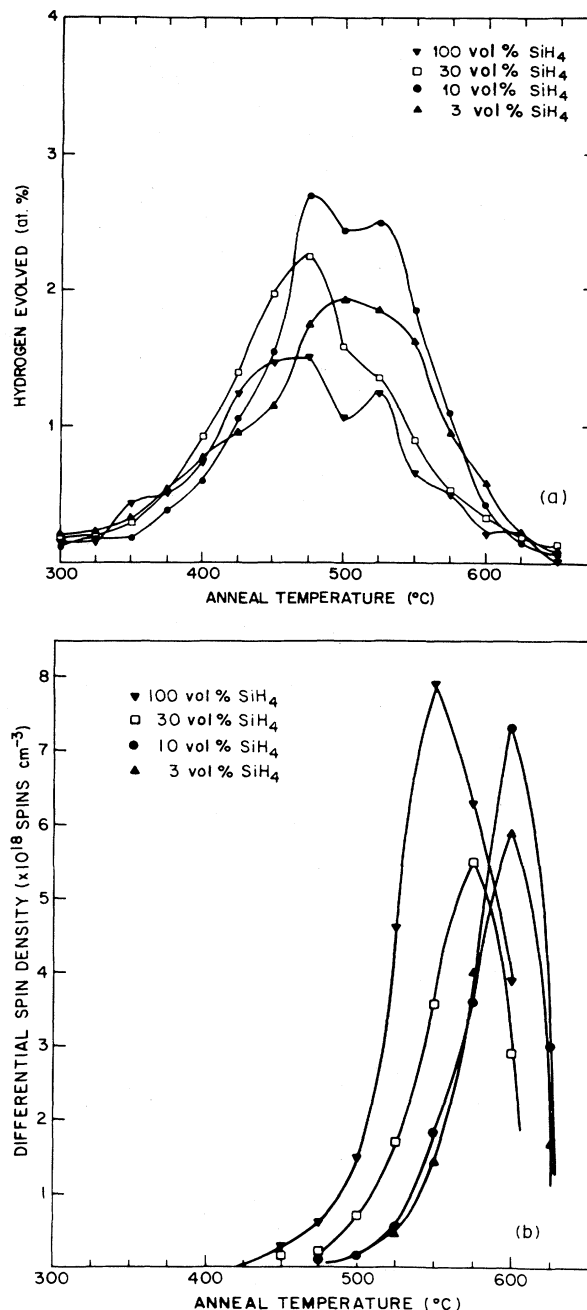


FIG. 1. (a) Atomic percent of hydrogen evolved at each progressive anneal temperature for four thin *a*-Si:H films ($d < 1.3 \mu\text{m}$). (b) Differential increase in spin density after each anneal for the same samples.

optical measurements presented here.

The hydrogen evolved during the anneal at each temperature was integrated into a measurement of the total evolved hydrogen density as a function of temperature. The data for the six *a*-Si:H samples studied are shown in Fig. 3. The total integrated hydrogen concentrations evolved from the various samples by annealing up to 650 or 675°C are summarized in Table I. Note that all six samples fall in the range from 10.1 to 20.8 at. % hydrogen.

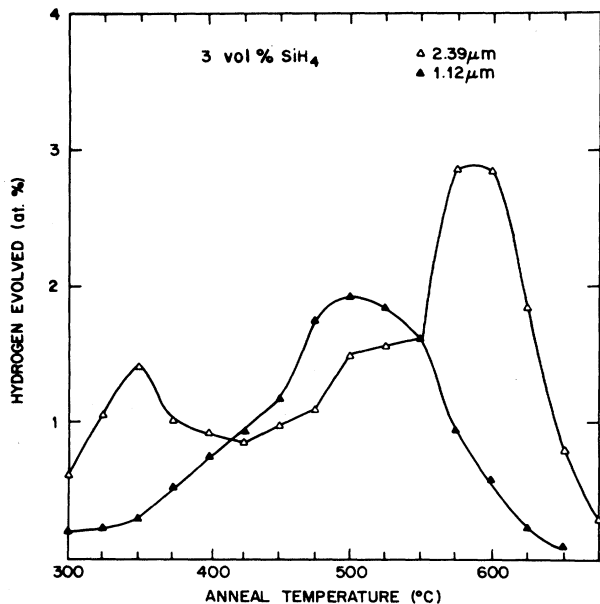


FIG. 2. Atomic percent of hydrogen evolved at each progressive annealing temperature for the two 3-vol % SiH_4 films, samples 5 and 6, which varied in thickness and growth rate.

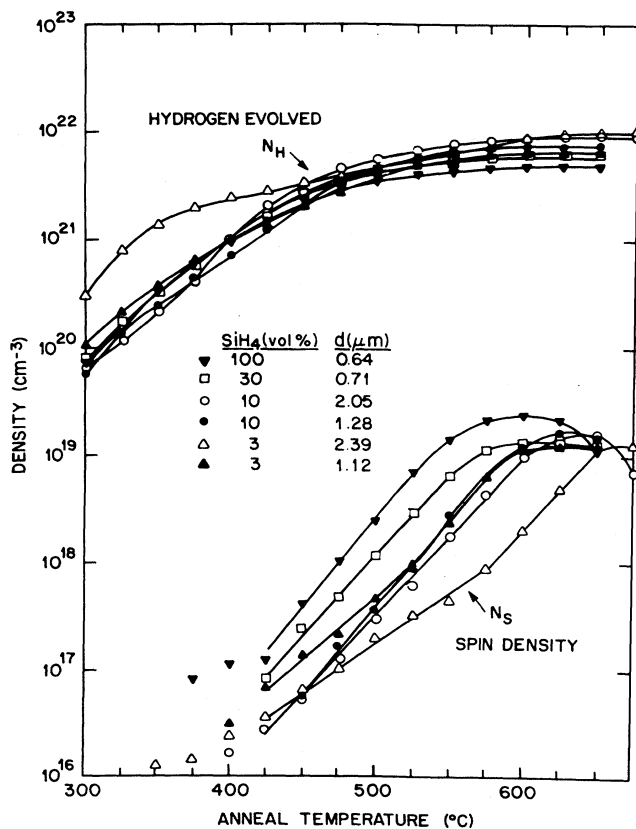


FIG. 3. Comparison of the cumulative densities of evolved hydrogen and spin formation.

The ESR parameters monitored in conjunction with the H evolution agree generally with measurements made in previous studies.^{1,3} After the 500°C anneal we observed a linewidth of approximately 5 G which decreased to about 4 G after the 650°C anneal. The *g* factor observed was typically near 2.006.

The cumulative ESR spin-density increases produced by the hydrogen-evolution heat treatments are also shown in Fig. 3. The spin signals for most samples annealed below 400°C were below the resolution limit of around 5×10^{11} spins (corresponding to a spin density of approximately 10^{16} cm^{-3}) despite a significant amount of hydrogen evolution. The spin density of samples grown with a 10-vol % or greater concentration of SiH_4 increased exponentially with temperature to around 550°C. Peak signals of approximately 1.5×10^9 spins cm^{-3} were observed at annealing temperatures near 625°C. Annealing at temperatures greater than 625°C produced a marked decrease in spin signal in the 100-vol % SiH_4 sample. This is assumed to result from structural changes such as the growth of microcrystallites. The spin signal of samples grown with 3 vol % SiH_4 increased more slowly and nonuniformly. A larger spin density was observed for samples grown with higher SiH_4 concentrations, yielding a maximum signal of 2.5×10^{19} spins cm^{-3} for the 100-vol % SiH_4 sample.

The differential increase in spin density as a function of annealing temperature is shown in Fig. 1(b) for the four thin samples. Note that the dominant spin signal increase occurs at the high-temperature side of the hydrogen-evolution peaks. Thus the release of hydrogen at lower temperature occurs without creation of states with unpaired electrons. This is consistent with the model of John *et al.*¹¹ in which the low-temperature evolution proceeds via the release of molecular hydrogen from regions of the film where bound hydrogen atoms are in close proximity. Such multiple defects may subsequently reconstruct to form spinless states in which all the electrons are paired.

A comparison of the net hydrogen content of the films and the maximum spin density created indicates that the two are inversely related, i.e., the maximum spin density is greater in samples that evolved less hydrogen. This is a surprising result. Hydrogen is generally believed to remove dangling-bond-like defects from *a*-Si; thus one might expect that the evolution of more hydrogen should uncover more defects. These results suggest that the dangling-bond density is not simply related to the amount of hydrogen evolved in the 500°C peak, but that both are more directly determined by the $[\text{SiH}_4]/[\text{Ar}]$ ratio during growth. On the other hand, discrepancies have been noted¹⁷ in highly hydrogenated films between the dangling-bond densities derived from the shoulder in the optical-absorption spectra and from ESR measurements. It has recently been suggested¹⁸ that in high-hydrogen-content films where dangling bonds may be in closer proximity, spin-spin interactions may reduce the sensitivity of the spin-resonance signal, leading to a systematic underestimate of the ESR-derived spin density in these materials. If this is the source of the trend observed in the cumulative spin density shown in Fig. 3, then we estimate slightly

more than an order of magnitude underestimate of N_s in the 10-vol % SiH_4 samples used in the optical measurements.

IV. EFFECTS OF ANNEALING ON THE OPTICAL PROPERTIES

A. Experimental results

In order to assess the effects of annealing on the optical properties of high-quality $a\text{-Si:H}$ films, eight of ten identical samples (i.e., films grown simultaneously) were each annealed at a single temperature in the range 300–600 °C. The results of ESR and hydrogen-evolution measurements for these samples, which are listed in Table II, fall within the range of values measured for the progressively annealed samples. The similarity in behavior indicates that a sample annealed progressively to a given maximum temperature is similar in net hydrogen evolution and spin density to a sample annealed *only* at the maximum temperature. In other words, the highest-temperature anneal has by far the greatest effect on the sample. This is consistent with the assumption of a range of hydrogen-bond energies E_B and escape rates that depend exponentially on the ratio E_B/kT . At a given temperature, the rates for a certain bond strength are just becoming significant, and all weaker bonds are rapidly broken, rendering the lack of previous lower-temperature anneals irrelevant. The 4-h anneal of sample 7F evolved more hydrogen and created a larger spin density than the 20-min anneal of sample 7E at the same temperature, causing effects more similar to the 20-min, 550 °C anneal. This pattern is reproduced throughout the optical data, indicating that the extended time compensated for the slower rates operant at the lower temperature.

Absorption spectra of these films reveal changes both in the position and shape of the absorption edge. As seen in Fig. 4, the low-energy shoulder becomes more prominent with annealing, extending almost to the highest measured values of the absorption coefficient α . As a result, the linear section in plots of $\sqrt{\alpha E}$ versus E typically used to

TABLE II. Results of ESR and hydrogen-evolution measurements.

Sample	Anneal temperature (°C)	Spin density (10^{17} cm^{-3})	Hydrogen evolved (10^{21} cm^{-3})	Hydrogen content (at. %)
7A		<0.1		20
7B		<0.1		20
7C	300	<0.1	0.7	18.6
7D	400	0.2	2.65	14.6
7E	500	1.6	5.3	9.4
7F	500 ^a	5.9	7.65	4.7
7G	525	3.7	6.0	8.0
7H	550	5.8	8.25	3.5
7I	570	14	8.2	3.6
7J	600	37	9.8	0.4

^aAnneal time 4 h. All others 20 min.

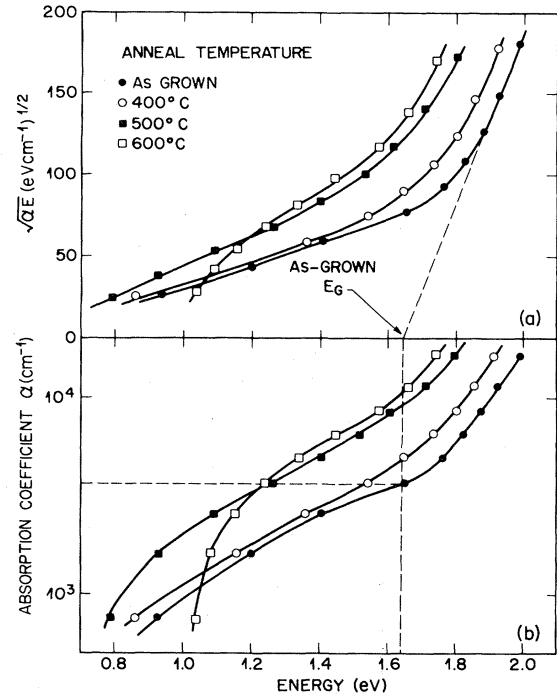


FIG. 4. Plots of the absorption coefficient α and $\sqrt{\alpha E}$ versus photon energy E . The optical gap of the as-grown sample, determined from the intercept of the linear fit in the high- α region, corresponds to $\alpha = 3.6 \times 10^3 \text{ cm}^{-1}$. The optical gaps of the annealed samples, which do not exhibit a clear linear region, are defined as the energies at which α attains this value.

define an optical gap, becomes overshadowed. The linear extrapolation for the as-grown sample yields a value of 1.64 eV for the optical gap, corresponding to $\alpha = 3.6 \times 10^3 \text{ cm}^{-1}$. For consistency, therefore, we define the optical gap E_G for the annealed samples as the energy at which α reaches this magnitude. This determination of E_G is still subject to interference from significant changes in the shape of the low-energy shoulder, and considerable uncertainty remains. Nevertheless, a clear trend is evident: E_G decreases steadily with anneal temperature. An alternative definition of E_G , such as E_{03} or E_{04} , i.e., the energy at which α is 10^3 or 10^4 cm^{-1} , respectively, slightly shifts the data to the higher or lower energy without disturbing this trend. In Fig. 5, E_G is plotted versus hydrogen content of the film.

The cw luminescence spectra are shown in Fig. 6. The peak energy, E_P , of the main luminescence band shifts from about 1.4 eV in sample 7A (as-grown) to about 0.95 eV in 7J (600 °C anneal). E_P is plotted versus hydrogen content in Fig. 5. The gap between E_G and E_P and the width of the spectra remain approximately constant across the range of annealing temperatures. Since E_G was measured at room temperature and E_P at 15 K, the difference $E_G - E_P$ includes the change in band gap between these two temperatures. The peak intensity of the main band is plotted versus spin density in Fig. 7(b).

An additional band is observed at about 0.7 eV in the annealed samples. Voget-Grote *et al.*⁶ have also reported

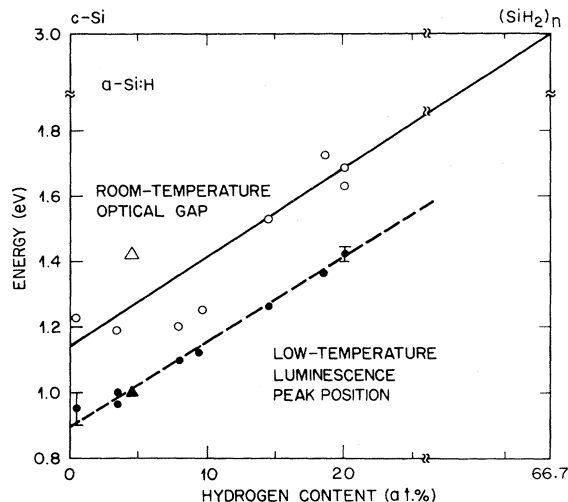


FIG. 5. Room-temperature optical gap and low-temperature luminescence-peak position versus hydrogen content of the films. The solid line is a linear fit between the 1.14-eV band gap of crystalline Si and the calculated (Ref. 21) 3.0-eV band gap of the fully polysilanated structure $(\text{SiH}_2)_n$. The circles represent 20-min anneals; the triangles represent 4-h anneals. The dashed line through the luminescence data is a guide to the eye.

a band in this region that is enhanced by annealing. Our data show that this band grows dramatically between 400 and 500°C anneal temperatures, reaching a maximum strength with the 525°C anneal. Higher-temperature an-

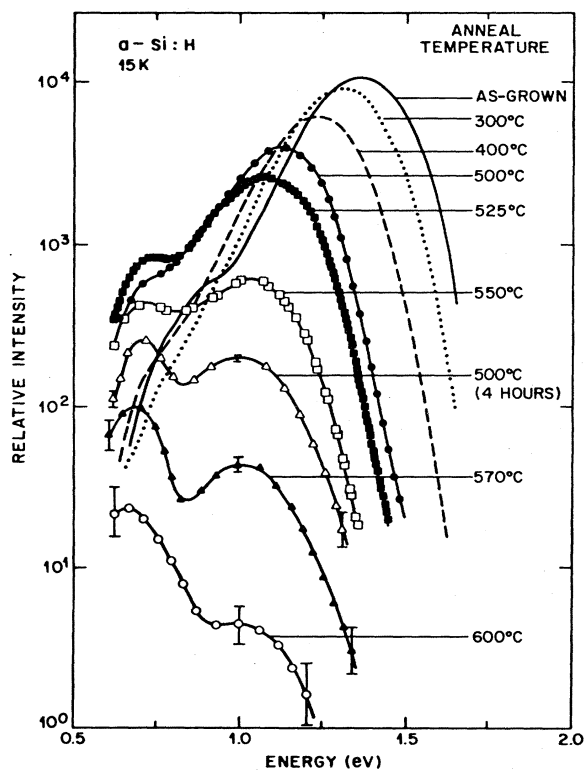


FIG. 6. Photoluminescence spectra as a function of anneal temperature. Error bars represent frequency-dependent scatter in the data.

neals, as well as the longer anneal at 500°C, reduce the strength of the band. This quenching is not as severe as for the main luminescence band, however, and at the highest anneal temperatures the 0.7-eV band dominates the spectrum. The peak intensity of this band is plotted versus spin density in Fig. 7(d). The peak position of this band does not shift perceptibly with anneal temperature.

Room-temperature Raman spectra were also taken to examine the extent of crystallinity in these annealed samples. Although the roughened substrates result in considerable diffuse scattering which interferes with sensitive Raman measurements, an upper limit of 1% could be placed on the extent of crystalline regions larger than ~ 50 Å in radius, even in the film annealed at 600°C.

The pulsed experiments reveal interesting changes with annealing in the PL decay statistics of the luminescence bands. In Fig. 8(a) the spectrally integrated intensity versus time of the main PL band is displayed for a subset of the samples. In Fig. 8(b) the data have been converted into a density of rates approximated¹⁹ by $G(t)=tI(t)$. From these two figures it is evident that a large part of the intensity loss is due to a competing nonradiative process which uniformly depletes all of the luminescing states. An additional loss mechanism occurs at later times. This is clear from the steeper slope and the drop in the density of rates at longer times in Figs. 8(a) and 8(b), respectively. To study these two loss mechanisms of the main luminescence band individually, we have measured the spectrally integrated intensities at 100 ns, well before the loss due to the slower process becomes significant. This allows us to isolate the effects of the early-time nonradiative process and to examine its dependence on anneal temperature and spin density. The 100-ns intensity of the main band is plotted versus spin density in Fig. 7(a).

Similar measurements of decay rates were made on the 0.7-eV band. The decay curves and density-of-rates distributions for luminescence energy, $E_{\text{PL}} < 0.78$ eV, are shown in Figs. 7(c) and 7(d). Since the response of the Ge detector falls in this region, spectrally integrated data tend to overemphasize contributions from the high-energy side of the band. As a result, there may be some interference from the tail of the main luminescence band that extends into the high-energy range of these measurements, especially in samples annealed at low temperatures where the main PL band still dominates the spectrum. The main trends with annealing evident in Fig. 8(d) are a rise of the entire distribution of rates followed by a fall which includes immediate and long-time quenching effects. As with the main PL band, the two quenching mechanisms are operative on very different time scales, allowing the effects of the fast process to be isolated by monitoring the intensity of 100 ns. The cw peak intensity and the spectrally integrated intensity of 100 ns are plotted versus spin density in Figs. 7(c) and 7(d).

Finally, the temperature dependence of the distribution of decay rates in the 0.7-eV band was measured for the sample annealed at 550°C. The results shown in Fig. 9 reveal that increased measurement temperature leads to an increase in both the fast and slow loss mechanisms, as with annealing. The late-time-scale loss is more severe, leaving only the 1- μ s peak by 175 K. The early-time sig-

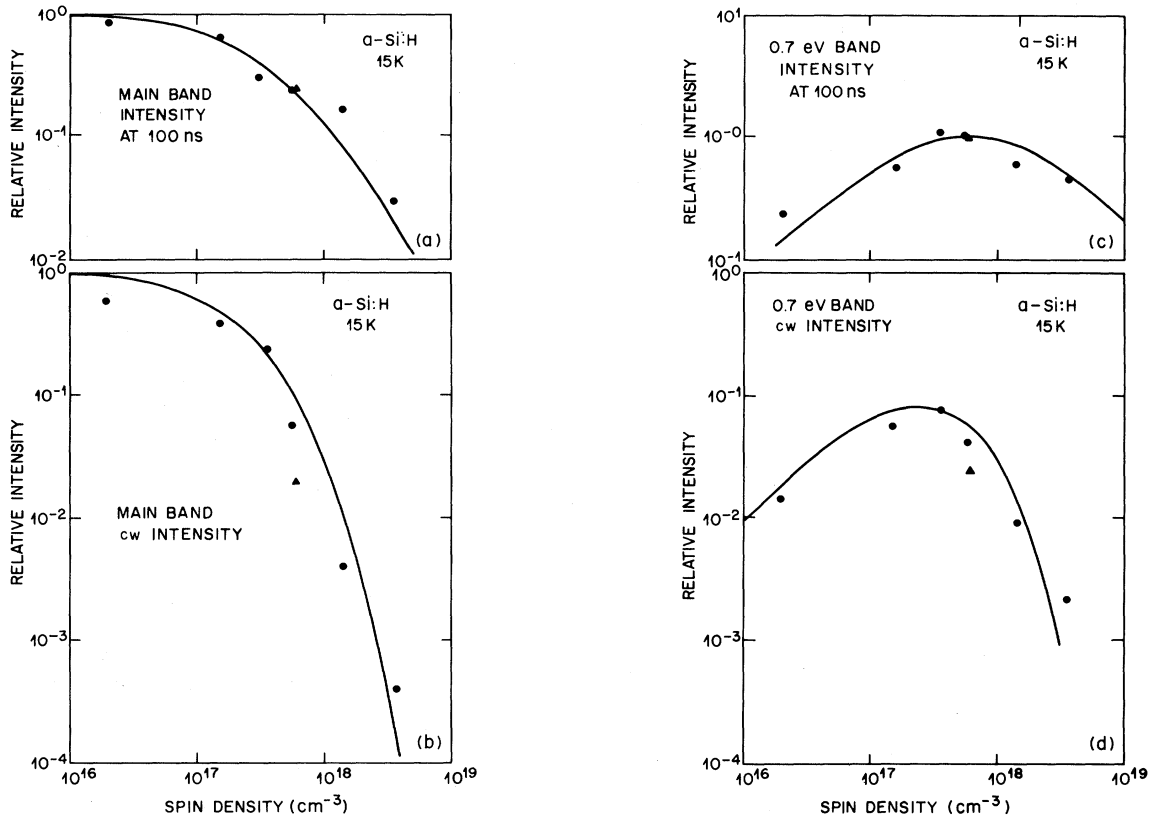


FIG. 7. Relative intensity in the main luminescence band (a) spectrally integrated at 100-ns delay, and (b) cw at the spectral peak. Equivalent data for the 0.7-eV band are shown in (c) and (d). The solid lines represent fits to the data. The 100-ns data are fitted with a simple branching-ratio formalism. For the cw efficiency the model combines the same initial branching ratio with subsequent tunneling to nonradiative recombination centers. Open circles represent samples annealed for 20 min; solid circles represent the sample annealed for 4 h.

nal only decays by about a factor of 2 across this temperature range. We have observed similar trends in the temperature dependence of the main PL band which also suffers increased losses both at early and late times at elevated temperatures,²⁰ the late-time losses being the more severe. The early-time quenching of the 0.7-eV band monitored at 100 ns is very similar to that of the main PL band in subnanosecond measurements of the same sample.²⁰ Both sets of data are shown in the inset of Fig. 9.

B. Discussion

The data of hydrogen evolution and spin density clearly show that single temperature anneals are, to first order, equivalent to progressive anneals up to the same maximum temperature. Thus, conclusions drawn from the two sets of annealing experiments may be interrelated. The cw absorption and luminescence data indicate a steady decrease of the optical gap with annealing temperature. Although some previous workers^{7,8} have reported similar monotonic behavior, reports on nonmonotonic relationships also appear in the literature.^{1,4} As suggested by deNeufville *et al.*,⁷ the nonmonotonic behavior may be associated with samples grown under nonideal conditions.

Our data strongly support this idea, and we propose that in addition to releasing hydrogen, annealing of nonideal films may promote some reconstruction of less stable defect sites and thus alter the character of the material. This is consistent with the data of Biegelsen *et al.*¹ in which all the samples grown well below 250°C exhibit a substantial decrease in the PL linewidth and spin density, and a large increase in PL efficiency when subjected to low-temperature anneals. It is significant that these changes bring the properties closer to the values observed in high-quality films. On the other hand, the single sample grown at 230°C reported in that study exhibits simple monotonic behavior consistent with our experiments.

Cody *et al.*⁹ have proposed that the shift of the absorption edge with hydrogen evolution reflects a broadening of the Urbach tail with increased disorder, rather than a narrowing of the band gap with varying alloy composition. Their absorption data clearly show a changing slope rather than a parallel shift of the absorption edge. Owing to the interference from the low-energy shoulder prominent in the absorption spectra of these samples, our absorption data do not distinguish between these two effects. We note, however, that while fairly low anneal temperatures (< 500°C) cause large spectral shifts, there is little loss in

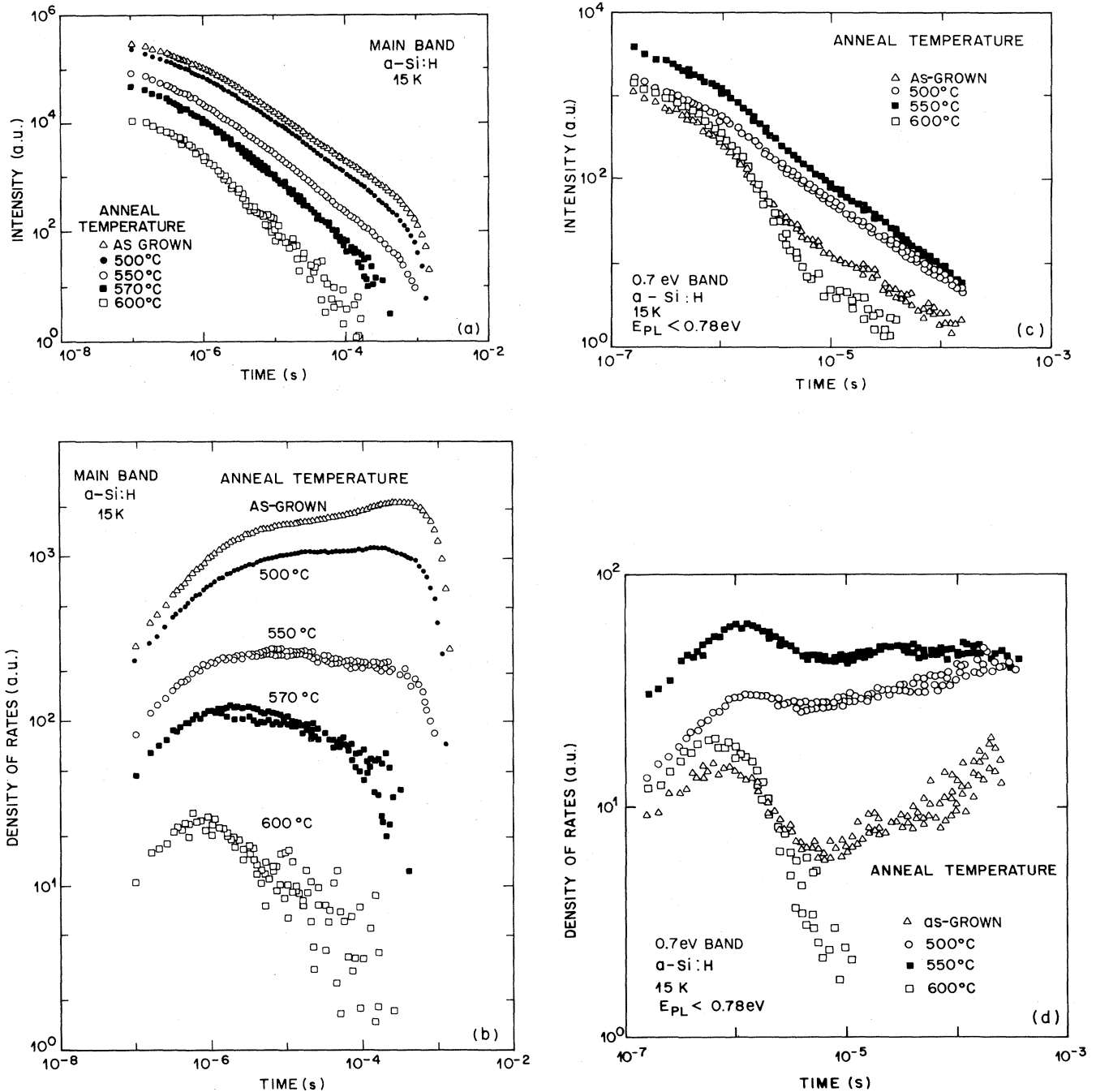


FIG. 8. (a) Decay of the spectrally integrated intensity and (b) density of rates in the decay of the main luminescence band. Equivalent data for the 0.7-eV band are shown in (c) and (d). The density of rates is approximated as the product of the delay and the intensity: $G(t) \sim tI(t)$.

quantum efficiency or increase in spectral width, effects which are usually associated with increased disorder. On the other hand, a simple linear dependence of the optical gap on alloy composition fits our data quite well, as shown in Fig. 5. The end points are the 1.14-eV band gap of crystalline Si and the 3.0-eV value calculated²¹ for the fully polysilinated structure, $(\text{SiH}_2)_n$. The parallel behavior of the more accurate and well-defined

luminescence-peak position of the main band further strengthens the credibility of the fit. These results suggest that, in the materials studied here, it is the alloy composition rather than disorder which is primarily responsible for the narrowing of the optical gap. Other recent work²² has also indicated a range of effects due to hydrogen in samples prepared by different techniques. Final resolution of this question must await further work on a variety

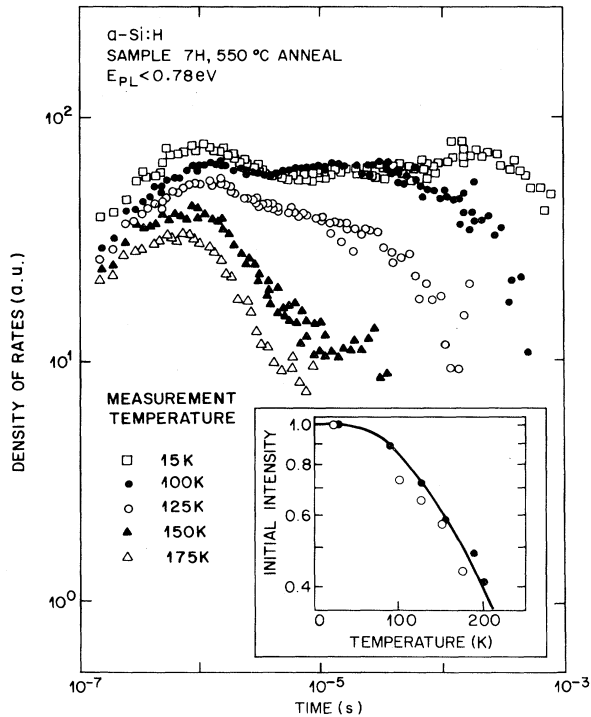


FIG. 9. Density of rates in the decay of the 0.7-eV PL band in sample 7H annealed at 550°C as a function of measurement temperature. The inset shows the temperature dependence of the 0.7-eV band intensity at 100-ns delay (open circles) superimposed on published data of the initial intensity in the main PL band (solid circles) measured in the same sample. The solid line is a fit assuming a competing multiphonon emission rate.

of materials.

While the main PL band tracks the observed absorption edge, the band at 0.7 eV does not. Photoelectron spectra^{23,24} indicate that it is primarily the valence band which is sensitive to hydrogen content, either directly or through disorder, while the conduction band is not, and neither are the energy levels of deep defects such as dangling bonds which are derived from mixtures of many bands. The absence of a shift in the 0.7-eV band position suggests that it does not involve the valence-band-tail states, but rather represents a transition between conduction-band-tail states and a deep defect, or possibly an internal transition at a defect. The observed shift of the main PL band, on the other hand, is consistent with its conventional identification as a band-tail-to-band-tail transition.

Previous reports of a low-energy PL band in annealed⁶ and ion- or electron-bombarded²⁵ materials suggested a correlation between the intensity of this band and the spin density N_s . The relationship is more clearly demonstrated by examining the ratio of the intensities in the 0.7-eV band and the main PL band as a function of N_s . A plot of this ratio versus N_s is shown in Fig. 10, and reveals a simple linear dependence over three decades. This linearity holds for both the cw data, which are absolute measurements, and for the 100-ns data, which have been normalized to the same magnitude. We conclude that a rapid branching process determines the initial populations with

a ratio proportional to N_s , and that the later quenching mechanism affects both bands similarly. These results led us to propose¹³ that both PL bands involve electrons trapped in conduction-band-tail states. Subsequent recombination with holes initially trapped in the valence-band tail results in the main band, and with holes trapped at dangling bonds, i.e., T_3^+ , results in the 0.7-eV band. We consider this model and its implications in more detail here.

First, we examine the early-time data in light of this model. Subnanosecond measurements of the main PL band²⁰ have shown that the initial loss mechanism is very rapid, < 100 ps, and that it increases exponentially with temperature. Photoconductivity measurements have found an analogous subpicosecond quenching of the initial photocurrent which exhibits the same activation energy. These combined results suggest a subpicosecond trapping process into deep traps, and the correlation with spin density observed here and in sputtered materials²⁶ implies that the relevant deep traps are dangling-bond defects.

In the simplest possible model of competing trapping mechanisms out of the photoexcited states, we consider only band-tail states and dangling-bond defects. Since in these undoped materials the majority of the dangling bonds are singly occupied in the ground state, i.e., T_3^0 , there are four dominant combinations for the initial trapping sites of the electrons and holes. The electron and hole can both be trapped in band-tail states, they can both be trapped at dangling bonds, the electron can be trapped at a dangling bond and the hole in a band-tail state, or, conversely, the electron can be trapped in a band-tail state and the hole at a dangling bond. Of these, only the first and last configurations, in which the electron is in a band-tail state, are likely to lead to luminescence within the spectral range of our experiments. Although the last

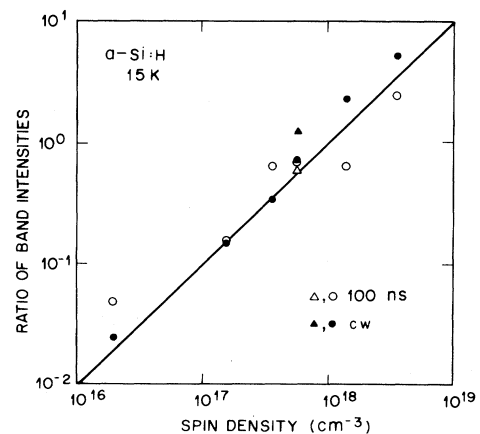


FIG. 10. Ratio of the intensity in the 0.7-eV band to that in the main band as a function of spin density. Solid symbols represent the cw peak intensity; open symbols represent the spectrally integrated intensity at 100-ns delay. Samples annealed for 20 min are shown as circles; the sample annealed for 4 h is shown by triangles. The solid line is a fit based on competing capture rates at band-tail and dangling-bond states, followed by tunneling of conduction-band-tail electrons to dangling-bond sites.

two are equivalent transitions for holes and electrons, the separation between the dangling-bond states and the valence band is expected to be smaller, especially in the samples annealed above 500°C (Refs. 23 and 24) where the hydrogen content is well below 10 at.%. Measurements of U , the energy needed to place the second electron on a dangling bond, lie in the range 0.1–0.2 eV in bulk *a*-Si:H (Ref. 27) and crystalline Si interfaces (Ref. 28). This places the recombination of a valence-band-tail hole and a T_3^- at or below about 0.6 eV for anneal temperatures above 500°C. Although this transition may be predominantly radiative at moderate anneal temperatures, it shifts rapidly to lower energy, tracking the shift of the valence-band edge, and we would not have observed it here. The transfer of an electron from a doubly occupied to an unoccupied dangling bond involves an even smaller transition energy, and is most likely nonradiative.

The initial populations of the two configurations which lead to the two observable PL bands may be calculated as a simple branching ratio. We make the assumptions that the densities of conduction- and valence-band-tail states, N_{BT}^e and N_{BT}^h , do not change grossly over this range of annealing temperatures, and that the excitation density is held sufficiently low to avoid saturating either the band-tail or dangling-bond states. We define

$$\alpha^e \equiv \frac{\nu_s^e}{\nu_{BT}^e N_{BT}^e}, \quad \alpha^h \equiv \frac{\nu_s^h}{\nu_{BT}^h N_{BT}^h},$$

where ν_s refers to the capture rate at a singly occupied dangling bond, ν_{BT} to an average capture rate at a band-tail state, and the superscripts e and h to electrons and holes, respectively. The fraction of photoexcited pairs trapped in the configuration leading to luminescence in the main PL band and in the band at 0.7 eV are then given by

$$f_{\text{main}} = \frac{\left[\frac{\nu_{BT}^e N_{BT}^e}{\nu_{BT}^e N_{BT}^e + \nu_s^e N_s} \right] \left[\frac{\nu_{BT}^h N_{BT}^h}{\nu_{BT}^h N_{BT}^h + \nu_s^h N_s} \right]}{1} = \frac{1}{(1 + \alpha^e N_s)(1 + \alpha^h N_s)}, \quad (1)$$

$$f_{0.7 \text{ eV}} = \frac{\left[\frac{\nu_{BT}^e N_{BT}^e}{\nu_{BT}^e N_{BT}^e + \nu_s^e N_s} \right] \left[\frac{\nu_s^h N_s}{\nu_{BT}^h N_{BT}^h + \nu_s^h N_s} \right]}{\alpha^h N_s} = \frac{\alpha^h N_s}{(1 + \alpha^e N_s)(1 + \alpha^h N_s)}. \quad (2)$$

We note immediately that this model predicts a ratio of populations, and thus band intensities, proportional to N_s , as observed. A linear fit to the ratio data of Fig. 10 yields $\alpha^h \sim 10^{-18} \text{ cm}^3$. Since the absolute scale of this ratio is set by the peak heights measured in the cw spectra, different line shapes of the two bands may result in an uncertainty in α^h on the order of a factor of 2. The fractional population calculated for the 0.7-eV band, Eq. (2), predicts an initial rise and subsequent fall of the intensity with N_s , with the peak occurring at $N_s = (\alpha^e \alpha^h)^{-1/2}$. The fit to the 100-ns data of Fig. 7(c) then yields $\alpha^e \sim 3 \times 10^{-18} \text{ cm}^3$. Finally, these parameters are used to fit the 100-ns intensity of the main PL band in Fig. 7(a).

The initial populations of two radiative configurations are also observed to be temperature dependent. The initial luminescence intensities decrease in unison above a low-temperature region in which they both saturate. The quenching of the main band has been modeled²⁰ as a thermally activated multiphonon emission process into a deep defect with a barrier height ~ 100 meV and a dominant coupling to ~ 38 -meV phonons. The fit to this model is shown as a solid line in the inset of Fig. 9. Within the branching-rate model presented here, the synchronous quenching of the 0.7-eV band implies that the temperature dependence of α^e is stronger than that of α^h , and thus that these fitting parameters describe the mechanism of electron capture at a singly occupied dangling bond.

The cw intensities of the two bands are affected by both early and late quenching mechanisms, and fall more rapidly with N_s than do the 100-ns intensities. The intensity ratio of the two bands remains proportional to N_s , however, implying that the late-time quenching mechanism is the same for both bands. Since both radiative transitions require an electron trapped in a conduction-band-tail state, these observations are consistent with the commonly assumed process of tunneling or diffusion of the electron to a singly occupied dangling-bond site, which then serves as a nonradiative recombination center. For this process to affect both bands similarly, the distribution of radiative recombination rates, with which this process competes, must also be similar. Since the slow quenching mechanism becomes significant at earlier times for larger N_s , the radiative contributions are best approximated by the data for low anneal temperatures. A comparison of the data shown in Figs. 8(b) and 8(d) indicates that the two radiative distributions are indeed comparable.

We apply the model of Street *et al.*²⁹ in which all electrons trapped in band-tail states within a critical radius R_c of a dangling bond are assumed to tunnel to the defect and recombine nonradiatively. This reduces the cw quantum efficiency by an additional factor, $\exp(-\frac{4}{3}\pi R_c^3 N_s)$. The analogous tunneling of the hole is likely to be less important because holes tend to be more deeply trapped and less mobile than electrons. The solid lines in Figs. 7(b) and 7(d) show fits of the combined quenching mechanisms on the cw efficiency of the two PL bands, yielding a consistent critical radius of 70 Å. This value is somewhat smaller than that typically obtained when only the tunneling is taken into account.²⁹

Previous attempts to identify the 0.7-eV band with a transition involving a dangling bond were called into question by optically detected magnetic resonance (ODMR) data,³⁰ which showed only a quenching signal at the dangling-bond resonance. We point out that our model is totally consistent with this result. The radiative transition from the conduction-band tail into an empty dangling bond is spin independent, so no microwave enhancement is expected. On the other hand, the spin-dependent transfer to a singly occupied dangling bond, which we postulate as leading to nonradiative recombination, provides an explanation of the quenching signal observed at the dangling-bond resonance.

The spectral data also tend to reinforce the model pro-

posed here. As discussed earlier, the shift of the main PL band with annealing and the absence of a similar shift of the 0.7-eV band are consistent with photoemission data^{24,25} on the effects of hydrogen content on the energy positions of the valence- and conduction-band edges. The 0.7-eV band is also noticeably narrower than the main band. While this may be, at least partially a reflection of the steeper Urbach tail of the conduction band, it is stimulating to speculate on the possibility suggested by Phillips³¹ that the dangling bonds lie primarily on internal surfaces. In this case, $2R_c$ would represent the average spacing between these surfaces. Such surfaces might be predominantly of one crystallographic orientation due to local growth kinetics, and/or less strained than typical bulk states, leading to a reduced inhomogeneous broadening of the linewidth. A very similar band has, in fact, been reported³² in crystalline Si which has been annealed following ion implantation at a dose sufficient to create a maximum defect luminescence intensity while leaving the crystal structure intact. Further annealing in atomic hydrogen quenches this band, strongly suggesting that it represents a transition involving dangling bonds. On the other hand, microcrystalline *a*-Si prepared without hydrogen by low-pressure chemical-vapor deposition exhibits a strong enhancement of luminescence in the 0.7-eV region following post-hydrogenation.³³

Low-energy PL bands in the (0.8–0.9)-eV region observed in doped *a*-Si:H (Refs. 34–36) are not generally narrower than the main PL band, and may have a different origin than the 0.7-eV band studied here. Street *et al.*³⁶ have recently reported bimolecular recombination kinetics and a very weak temperature dependence of these bands which clearly distinguish their behavior from that of the 0.7-eV band reported here. While these bands also appear to be correlated with an ESR signal at the position of the dangling-bond resonance, it is possible that dopant complexes containing a dangling bond are responsible. Further work on annealed, doped materials is underway in our laboratory to resolve this question.

It is useful to compare the optical results presented here with other types of measurements in *a*-Si:H. Photoinduced absorption (PA) is thought to be due to absorption by photoexcited holes. Thus transient PA provides complementary data on the density of holes remaining as a function of delay after pulsed excitation. The lack of large subpicosecond losses in picosecond PA measurements,³⁷ and the long decay times of PA signals in poor-quality samples with large spin densities,³⁸ preclude rapid recombination at dangling-bond sites, but are consistent with the rapid trapping postulated here, as long as the absorption cross sections for holes in band-tail states and dangling bonds are comparable. This interpretation implies that the PA decay at later times is not due to trapping at dangling bonds as suggested,³⁸ but rather to the subsequent nonradiative recombination at these sites in conjunction with losses due to radiative recombination. In high-defect-density materials the long-lived radiative components are short-circuited by faster nonradiative channels and the decay of radiative-state populations are rapid. The PA decay rate, however, remains slow. Thus, the long-delay PA decay must be dominated by nonradia-

tive recombination processes. This is consistent with recently reported careful comparisons of PL and PA dynamics in the same sample.³⁹

Comparisons with transport experiments are also important. In particular, time-of-flight (TOF) data provide an alternate measure of capture rates at band-tail states and dangling bonds. Measurements on low-⁴⁰ and high-spin-density⁴¹ materials interpreted within a dispersive transport picture provide values of $\nu_{BT}N_{BT}$ and ν_s , respectively. The room-temperature values obtained from these measurements predict trapping fractions at dangling bonds to be about 2 orders of magnitude smaller than those obtained here, and to obey a power-law temperature dependence.⁴² The comparison is complicated, however, by the longer-time scale of the transport measurements, where it is not possible to isolate any initial trapping processes from subsequent diffusion-controlled trapping. Nevertheless, if the later trapping at dangling bonds occurs through thermal excitation to extended states above the band edge, then the relative capture rates of band-tail states and dangling bonds obtained from transport data might be expected to agree with those for the initial photoexcited state calculated from our PL data. We note that one possibility for the discrepancy is our ESR determination of N_s , which, as discussed earlier, may underestimate the actual spin density by more than an order of magnitude and thus overestimate α^e and α^h by the same factor. Further support for this argument is found in other reports of the low-energy PL band in annealed⁶ and bombarded²⁵ *a*-Si:H. Those samples which were prepared at 100 vol % SiH₄ exhibit peak intensities of this band at spin densities more than an order of magnitude higher than reported here. A final resolution of this question must await further work.

V. SUMMARY

In this paper we have examined the effect of isochronal annealing on the optical properties, spin density, and hydrogen evolution of high-quality *a*-Si:H films. Under progressive annealing, thin films grown under near-optimal conditions exhibit a single peak in differential hydrogen evolution at about 500°C. The peak in spin creation occurs at a somewhat higher temperature, indicating that only the most tightly bound hydrogen leaves behind dangling bonds that cannot reconstruct into spinless configurations. Similar patterns of hydrogen evolution and spin creation are observed in the second set of annealing experiments where identical samples were annealed at single temperatures. Evidently, the highest-temperature anneal of a series is the prime determinant of film properties.

In general, we find the changes in the optical properties in these high-quality films to be much more straightforward than reported previously for films grown under a range of conditions far from optimal.¹ The reason for this difference may well be that the first effect of annealing on nonoptimally produced films is to allow some reconstruction of the structure to more closely resemble good material. Only later do the opposing effects due to

hydrogen evolution become apparent, resulting in non-monotonic behavior. Thus, by focusing solely on the behavior of high-quality films, the effects of hydrogen evolution are more effectively isolated, and can be more clearly examined.

The optical gap monitored both by absorption and luminescence measurements decreases steadily as hydrogen is evolved. When the gap is plotted versus hydrogen concentration, we find the values to be consistent with a straight-forward fit between crystalline silicon at one end and the calculated value²¹ for a fully polysilanated structure at the other end. This result suggests that in some cases alloy composition may be the major determinant of the optical gap rather than disorder, as previously suggested.⁹

The cw luminescence spectra exhibit two PL bands: the main band which shifts to lower energy and quenches monotonically with anneal temperature, and a narrower band at 0.7 eV which does not shift noticeably and first grows and then quenches with anneal temperature. The ratio of intensities in the two bands scales linearly with spin density, suggesting an involvement of the dangling-bond states in the 0.7-eV band. Time-resolved measurements of the decay rates indicate an initial loss mechanism that determines the absolute and relative populations of the two sets of luminescing states, followed much later ($\geq 1 \mu\text{s}$) by additional quenching that affects both bands similarly. Both quenching processes correlate with spin density.

We discuss in detail a self-consistent model of these results¹³ in which the main PL band originates from band-tail-to-band-tail transitions, and the 0.7-eV band is due to the recombination of electrons trapped in band-tail states and holes trapped at dangling bonds. The initial populations in dangling-bond and band-tail states reflect the outcome of the competition between these states for initial capture of the photoexcited carriers. These popula-

tions are calculated using a simple branching-ratio model of the relative capture rates which correctly predicts the spin-density dependence of the early-time intensities in the two PL bands. The slower quenching process is modeled as tunneling of band-tail electrons to singly occupied dangling-bond sites where they subsequently recombine nonradiatively, or at least do not emit radiation within our range of detection. This picture is consistent with published ODMR data which reveal only a quenching signal in the 0.7-eV band at the dangling-bond resonance.³⁰ The initial intensities of the two bands fall in unison with temperature above a saturated region. We interpret this quenching process as being due to thermally activated trapping of the electrons at dangling-bond sites via a multiphonon emission process.

These results have been compared with other data in the literature. Our model identifies fast trapping rather than fast recombination as the initial loss mechanism. This is consistent with PA results in which there is no fast signal decay,³⁸ if we assume that the absorption cross section for holes in band-tail and dangling-bond states are comparable. Although TOF data^{40,41} provide values for the relative trapping rates which are not in agreement with those measured here, a direct comparison of the data is not possible because the transport measurements do not isolate fast and slow trapping processes. It is also possible that the apparent discrepancy could be the result of an underestimate of N_s in our samples. Finally, we note that recent experiments in the (0.8–0.9)-eV bands observed in doped materials reveal quite different characteristics,³⁶ suggesting a different origin for these bands.

ACKNOWLEDGMENTS

We thank K. Lyons and T. Negran for the Raman scattering measurements, and J. C. Phillips and D. V. Lang for useful discussions.

¹D. K. Biegelsen, R. A. Street, C. C. Tsai, and J. C. Knights, *Phys. Rev. B* **20**, 4839 (1979).

²H. Fritzsche, M. Tanielian, C. C. Tsai, and P. J. Gaczi, *J. Appl. Phys.* **50**, 3366 (1979).

³R. A. Street, J. C. Knights, and D. K. Biegelsen, *Phys. Rev. B* **18**, 1880 (1978).

⁴A. Deneuve, A. Mini, and J. C. Bryère, *J. Phys. C* **14**, 4531 (1981); *J. Appl. Phys.* **50**, 3366 (1979).

⁵K. J. Matysik, C. J. Mogab, and B. G. Bagley, *J. Vac. Sci. Technol.* **15**, 302 (1978).

⁶U. Voget-Grote, W. Kümmerle, R. Fischer, and J. Stuke, *Philos. Mag.* **B 41**, 127 (1980).

⁷J. P. deNeufville, T. D. Moustakas, and A. F. Ruppert, *J. Non-Cryst. Solids* **35-36**, 481 (1980).

⁸E. C. Freeman and W. Paul, *Phys. Rev. B* **18**, 4288 (1978).

⁹G. D. Cody, T. Tiedje, B. Abeles, B. Brooks, and Y. Goldstein, *Phys. Rev. Lett.* **47**, 1480 (1981).

¹⁰K. Zellama, P. Germain, S. Squelard, B. Bowdan, J. Fontenille, and R. Danielou, *Phys. Rev. B* **23**, 6648 (1981).

¹¹P. John, I. M. Odeh, M. J. K. Thomas, M. J. Tricker, F. Ridoch, and J. I. B. Wilson, *Philos. Mag.* **B 5**, 671 (1980).

¹²J. C. Knights and R. A. Lujan, *Appl. Phys. Lett.* **35**, 244

(1979).

¹³B. A. Wilson, A. M. Sergent, and J. P. Harbison, *Phys. Rev. B* **30**, 2282 (1984).

¹⁴J. P. Harbison, A. J. Williams, and D. V. Lang, *J. Appl. Phys.* **55**, 946 (1984).

¹⁵H. Dersch, J. Stuke, and J. Beichler, *Appl. Phys. Lett.* **38**, 456 (1981).

¹⁶D. L. Staebler and C. R. Wronski, *Appl. Phys. Lett.* **31**, 292 (1977).

¹⁷S. Yamasaki, N. Hata, T. Yoshida, H. Oheda, A. Matsuda, H. Okushi, and K. Tanaka, *J. Phys. C* **4**, 297 (1981).

¹⁸G. Cody (private communication).

¹⁹G. S. Higashi and Marc Kastner, *Philos. Mag.* **B 47**, 83 (1983).

²⁰B. A. Wilson, P. Hu, J. P. Harbison, and T. M. Jedju, *Phys. Rev. Lett.* **50**, 1490 (1983); B. A. Wilson, P. Hu, J. P. Harbison, and T. M. Jedju, *Phys. Rev. B* **28**, 5901 (1983).

²¹Douglas C. Allan and J. D. Joannopoulos, *Phys. Rev. Lett.* **44**, 43 (1980).

²²N. Maley and J. S. Lanin, *Bull. Am. Phys. Soc.* **29**, 425 (1984).

²³B. von Roedern, L. Ley, and M. Cardona, *Phys. Rev. Lett.* **39**, 1576 (1977).

- ²⁴B. von Rodern, L. Ley, and F. W. Smith, in *Proceedings of the 14th International Conference on the Physics of Semiconductors, Edinburgh, 1978*, edited by B. L. H. Wilson (IOP, Bristol, 1978), p. 701.
- ²⁵R. Street, D. Biegelsen, and J. Stuke, *Philos. Mag. B* **40**, 451 (1979).
- ²⁶R. W. Collins, P. Viktorovitch, R. L. Weisfield, and William Paul, *Phys. Rev. B* **26**, 6643 (1982).
- ²⁷J. D. Cohen, J. P. Harbison, and K. W. Wecht, *Phys. Rev. Lett.* **48**, 109 (1982).
- ²⁸M. C. Chen and D. V. Lang, *Bull. Am. Phys. Soc.* **29**, 339 (1984).
- ²⁹R. A. Street, J. C. Knights, and D. K. Biegelsen, *Phys. Rev. B* **18**, 1880 (1978).
- ³⁰M. Yoshida and K. Morigaki, in *Proceedings of the 10th International Conference on Amorphous and Liquid Semiconductors, Tokyo, 1983*, edited by K. Tanaka and T. Shimizu (North-Holland, Amsterdam, 1983), p. 357.
- ³¹J. C. Phillips, *Phys. Status Solidi B* **101**, 437 (1980); *Phys. Rev. Lett.* **42**, 1151 (1979).
- ³²J. I. Pankore and C. P. Wu, *Appl. Phys. Lett.* **35**, 937 (1979).
- ³³F. Boulitrop and A. Chenevas-Paule, *Solid State Commun.* **48**, 181 (1983).
- ³⁴R. A. Street, *Adv. Phys.* **30**, 593 (1981), and references therein.
- ³⁵W. Rehm, D. Engemann, R. Fischer, and J. Stuke, in *Proceedings of the 13th International Conference on the Physics of Semiconductors*, edited by F. G. Fumi (North-Holland, Amsterdam, 1976), p. 525.
- ³⁶R. A. Street and D. K. Biegelsen, *Bull. Am. Phys. Soc.* **29**, 507 (1984).
- ³⁷Jan Tauc, in *Festkörperprobleme, Vol. XXII of Advances in Solid State Physics*, edited by J. Treusch (Vieweg, Braunschweig, 1982), p. 85.
- ³⁸Douglas R. Wake and Nabil M. Amer, *Phys. Rev. B* **27**, 2598 (1983).
- ³⁹H. A. Stoddart, D. Pfof, Z. Vardeny, and J. Tauc, *Bull. Am. Phys. Soc.* **29**, 507 (1984).
- ⁴⁰T. Tiedje, J. M. Cebulka, D. L. Morel, and B. Abeles, *Phys. Rev. Lett.* **46**, 1425 (1981).
- ⁴¹R. A. Street, *Appl. Phys. Lett.* **41**, 1060 (1982).
- ⁴²R. A. Street, *Philos. Mag. B* **49**, 215 (1984).